*Article*

# On Mineral Retrosynthesis of a Complex Biogenic Scaffold

**Ashit Rao [1,2,*], José L. Arias [3,*] and Helmut Cölfen [2]**

[1] Freiburg Institute for Advanced Studies, Albert Ludwigs University of Freiburg,
79104 Freiburg im Breisgau, Germany
[2] Physical Chemistry, Department of Chemistry, University of Konstanz, 78464 Konstanz, Germany;
helmut.coelfen@uni-konstanz.de
[3] Faculty of Veterinary Sciences, University of Chile, 88208-08 Santiago, Chile
[*] Correspondence: ashit.rao@frias.uni-freiburg.de (A.R.); jarias@uchile.cl (J.L.A.)

**Abstract:** Synergistic relations between organic molecules and mineral precursors regulate biogenic mineralization. Given the remarkable material properties of the egg shell as a biogenic ceramic, it serves as an important model to elucidate biomineral growth. With established roles of complex anionic biopolymers and a heterogeneous organic scaffold in egg shell mineralization, the present study explores the regulation over mineralization attained by applying synthetic polymeric counterparts (polyethylene glycol, poly(acrylic acid), poly(aspartic acid) and poly(4-styrenesulfonic acid-*co*-maleic acid)) as additives during remineralization of decalcified eggshell membranes. By applying $Mg^{2+}$ ions as a co-additive species, mineral retrosynthesis is achieved in a manner that modulates the polymorph and structure of mineral products. Notable features of the mineralization process include distinct local wettability of the biogenic organic scaffold by mineral precursors and mineralization-induced membrane actuation. Overall, the form, structure and polymorph of the mineralization products are synergistically affected by the additive and the content of $Mg^{2+}$ ions. We also revisit the physicochemical nature of the biomineral scaffold and demonstrate the distinct spatial distribution of anionic biomolecules associated with the scaffold-mineral interface, as well as highlight the hydrogel-like properties of mammillae-associated macromolecules.

**Keywords:** biomineral; calcium carbonate; crystallization; egg; polymer; liquid precursor; mineralization; scaffold

## 1. Introduction

In higher organisms, biomineralization involves an efficacious integration of inorganic building units with an organic scaffold to yield functional materials [1–3]. The architecture and structure-property relationships exhibited by biominerals inspire synthetic counterparts due to fascinating materials emerging from bottom-to-top routes under physiological conditions [4–6]. Several complex biominerals present an organic scaffold (or matrix), which plays a crucial role in regulating mineral growth by incorporating inorganic precursors, such as ions, ion-clusters and amorphous phases. For instance, in nacre and bone material, the physicochemical properties of the scaffold tune interactions with mineral precursors and subsequently lead to hierarchically-organized composite biominerals [3,7,8]. Thus, the niche conditions of crowding and confinement presented by the scaffold offer a defined physicochemical environment towards mineralization reactions [9,10]. In biological environments, the activity of nucleation and crystallization additives modulate mineral growth. The dynamism of additives with respect to conformation, charge, molar mass, self-association propensity and phase behavior in relation to the distinct stages of material formation are crucial for

regulating biomineralization [10–15]. From this view, the cooperation of scaffolds and biomolecular additives provides an exceptional control over mineralization in Nature.

The avian shell is a multifunctional biomineral with material properties that are evolutionarily optimized for protection, hatchability and diffusion [16–20]. Identified as one of the most rapid forms of calcification in Nature, the avian egg plays a key role in several disciplines, such as archaeology and paleontology, as well as art and philosophy [21]. Structurally, the shell is a multi-layered calcitic bioceramic. As the egg migrates through the oviduct, the biomineral matures under the influence of biomolecular additives and an extracellular matrix [22–24]. The matrix, primarily composed of collagen fibers, constitutes the shell membranes. Each fiber exhibits a core surrounded by a glyco-proteinous material termed as the mantle. This serves as the interface with the inorganic phase [25]. During mineral growth, crystals nucleate on the outer side of the shell membrane at specific sites called mammillae. This organic matrix enables the formation of a calcified layer (i.e., palisade) composed of calcite columns [26]. Morphologically, the palisade zone exhibits three regions (cone, middle and vertical layers) that vary with respect to relative crystallographic orientation. The outermost layer, the cuticle, is composed of glycoproteins, pigments in the colored eggs and hydroxyapatite. This composite shell microstructure reflects a sophisticated spatiotemporal regulation of nucleation and crystal growth, acquired synergistically via an organic scaffold and biomolecular additives [22].

The complexity of egg shell formation is reflected by proteomic studies, which report several biomolecules (>500 mineral-associated uterine fluid proteins), the relative abundance of which depends on the calcification stage [27,28]. These biomolecules are classified on the basis of their primary function as direct regulators of nucleation and crystal growth, antimicrobial agents, as well as biomolecular checkpoints for protein folding and proteolysis. Among direct regulators of nucleation and crystal growth, interwoven collagen fibrils of the shell membrane and certain associated proteins inhibit crystal nucleation, whereas the mammillae constituents present sites for mineralization [16,23,29]. From this perspective, mammillae-associated keratan sulfate proteoglycans exhibit anionic properties optimal for calcium binding and promote the nucleation of less soluble phases (i.e., crystalline) of $CaCO_3$ [30]. Present in the shell matrix of the palisade, ovoglycan, a proteoglycan contains a core protein, ovocleidin-116 and presents glycosaminoglycan chains of dermatan sulfate [31]. Isolated from the mineral phase, dermatan sulfate proteoglycans induce highly soluble phases of $CaCO_3$, which suggests a role in the transport of mineral precursors and crystal formation [30,32]. Another biomacromolecule associated with the scaffold is ovocleidin-17, an abundant constituent of the shell matrix with a C-type lectin-like domain [33]. This particular domain is suggested to be important in other biomineralization systems, such as the sea urchin spine [13]. Osteopontin, a protein ubiquitous in biological calcification processes is shown to interact with the {104} calcite face and inhibit mineral deposition in relation to distinct stages of shell development [34,35]. These studies collectively show that biomacromolecules in the shell matrix and membrane synergistically operate to produce the final bioceramic material. Although the exact function of individual biomolecules in the mineralization cascade is not clear, the homology among biomolecules within the shell material of different species suggests a minimal toolbox essential for egg shell development. With established biochemical functions in the mineralization process, macromolecules also encompass physicochemical purposes as molecular materials. The topological distribution of the mineral nucleation sites (mammillae) on the shell membrane lead to anisotropic crystal growth and elongated structures (palisade) due to spatial constraints towards the growing mineral [17,32]. On these lines, the excluded volume effect and spatial confinement at distinct length scales within the biomineral scaffold significantly impact mineral growth and structure [10]. For a heterogeneous biomineral scaffold, such as that in the egg shell, macromolecular composition itself provides distinct mechanical features. With material composition similar to the egg shell scaffold, cartilaginous tissue is generally rich in proteoglycans and collagen [36]. The proteoglycans being polyelectrolytes of high charge density provide a high osmotic pressure and imbibe water, maintaining turgor. On the other hand, the collagen network presents tensile properties and resists swelling. The resulting composite material exhibits a combination of good flexibility and

high tensile strength [36]. In a similar manner, during egg shell development, the macromolecular properties of mineralization additives can modulate material properties, in addition to their primary purpose of regulating mineralization. This suggests co-operative relationships between the mineral scaffold and crystallization additives towards shaping the structure, as well as defining material properties of the composite biomineral.

Studies focusing on biomimetic materials have attempted to replicate the form and structure of natural materials by applying bio-inspired strategies. For instance, mineralization of collagen in the presence of poly(acrylic acid) (PAA), a synthetic anionic polymer, leads to a hierarchical composite structure similar to natural bone tissue [37]. The polymer-induced liquid precursor (PILP) phase stabilized by PAA exhibits liquid-like properties and is suggested to be drawn into the gaps within collagen fibrils by capillary effects. On crystallization, the collagenous matrix encloses organized assemblies of hydroxyapatite nanoparticles formed on phase transformation [38]. Mineralization of the insoluble matrix of nacre material in the presence of PAA also reports morphologies structurally analogous to the natural biomineral [39]. These studies demonstrate the crucial role of anionic biomacromolecules in determining non-equilibrium crystal morphologies and hierarchical structures that are typical of natural composite biominerals. Even in the case of egg shell formation, sulfated biopolymers appear to modulate biomineralization by inducing transient stabilization of liquid-like mineral precursors. Supporting evidence comes from the effects of an egg shell associated biomacromolecule, dermatan sulfate, which leads to transient mineral phases with considerably higher solubility products than that of solid amorphous calcium carbonate (ACC) [30]. Combined with carbonic anhydrase, dermatan sulfate produces calcite crystals with a columnar morphology, similar to the natural biomineral [32]. A chemically-similar anionic polysaccharide, dextran sulfate, leads to coacervates formed via a phase separation process in the course of mineralization [40]. Studies applying soluble components of the egg organic matrix also report the transient stabilization of amorphous mineral precursors with the involvement of $Mg^{2+}$ ions [41]. Along these lines, the level of magnesium incorporation in the eggshell is suggested to correlate with the distribution of organic content across different species (subject to factors such as bird age) [42]. Although a cooperative function of $Mg^{2+}$ ions and organic additives during biomineralization is under investigation, the impact of $Mg^{2+}$ ions as a co-additive species on mineral nucleation and crystal growth was recently demonstrated [43–45].

Given the heterogeneous composition and structure of the egg shell scaffold, the cooperation between the biomineral scaffold, crystallization additives and mineral precursors emerges as a fundamental aspect of the biomineralization process. The complementarity between the physicochemical nature of transient mineral precursors and mineral matrices has also been suggested [10]. Therefore, in this study, we seek to (i) revisit the distribution and physical nature of organic macromolecules constituting the egg shell scaffold using the tools of microscopy and (ii) explore the relation between distinct mineral precursors and the biomineral matrix by applying synthetic additives during the ex situ mineralization of decalcified egg membranes. We show that the properties of polymeric additives, such as molar mass and charge distribution, as well as the content of $Mg^{2+}$ ions affect mineralization in terms of structure and polymorph. Interactions between transient mineral precursors and the organic matrix are shown to be modulated by a complex mineralization environment, which involves the hydrogel properties of mammillae-associated macromolecules, as well as synergetic relations between organic additives and $Mg^{2+}$ ions. In this manner, the physicochemical properties of the biomineral scaffold are evolutionary optimized for achieving homeostatic biomineralization.

## 2. Results and Discussion

### 2.1. Architecture of the Organic–Inorganic Interface

During the initial stages of eggshell development, mammillae, i.e., protrusions associated with the collagenous matrix, serve as important sites for regulating mineral nucleation [16,29,32].

The distribution of mammillae and organic constituents of the scaffold affect structural aspects, such as mammillary cone size, palisade morphology, as well as mechanics of the bioceramic [46,47]. To gain a better insight, morphological features of the shell layers are revisited by applying tools of microscopy. After decalcification-based separation of the membrane and mineral layers, the inner surfaces of the shell exhibit remnants of the mammillae constituents co-localized with cone-shaped initial mineral deposits (Figure 1A, arrows). After the removal of this organic matter by calcination, the spaces occupied by mammillae residues exhibit distinct microporous networks extending into the palisade superstructure (Figure 1B, arrows). This suggests an interlocking of the scaffold with the palisade cones at mammillae sites, serving as a robust interface between the organic and inorganic layers of the mature biomineral.
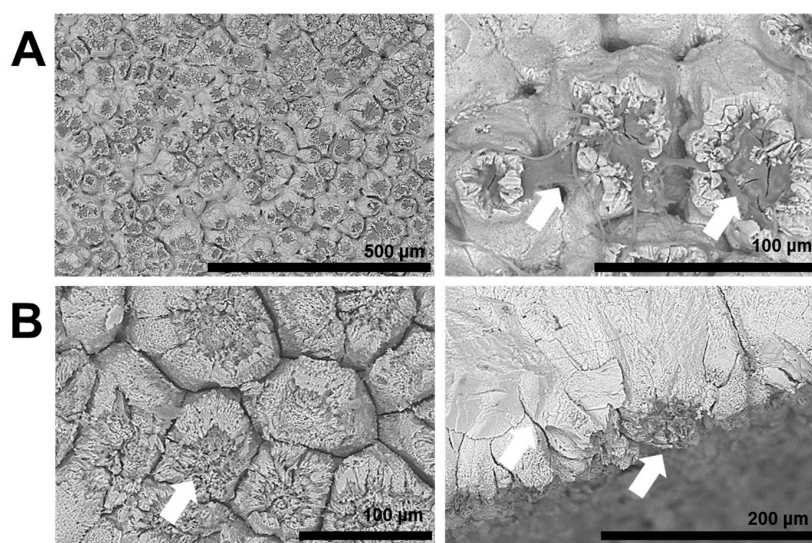


**Figure 1.** Representative SEM images of inner surfaces of the egg shell (**A**) before and (**B**) after calcination. Arrows indicate (**A**) co-association of mammillae content with the palisade base and (**B**) high porosity of the palisade cone after calcination.

Several studies have revealed the important functions of anionic proteoglycans during egg shell development [32,48]. To explore the distribution of biomacromolecules at the mineral-scaffold interface, the inner shell surface and outer surface of the scaffolding membrane are probed using glycan-selective stains. Using Congo red, a diazo stain with a broad affinity towards β-glucans, the membrane-associated collagen fibrils, as well as mammillae are stained orange, suggesting respective compositions rich in β-glucan-based polysaccharides (Figure 2A). This agrees with the reported abundance of proteins post-translationally modified with glycan residues, as well as anionic polysaccharides in the eggshell structure [32,48,49]. As the inner shell surfaces exhibit β-glucan enrichment specifically at the mammillae residues, the role of proteoglycans in the interlocking of organic and inorganic layers is suggested (Figure 1).

To specifically probe the distribution of sulfated glycosaminoglycans (sGAGs), the shell and membrane surfaces are stained using 1,9-dimethyl-methylene blue (DMMB) (Figure 2B). Due to the metachromasic property of DMMB, areas of the shell and membrane rich in sGAGs are stained either pink or purple. The egg membrane is extensively stained by DMMB, independent of mammillae distribution (Figure 2B). This suggests an abundance of sGAGs in association with the mammillae, as well as the collagenous mesh of the egg membrane. On the other hand, the inner surface of the shell is selectively stained at the mammillae (Figure 2B). The co-association of sGAGs with the shell surface suggests that these anionic biomacromolecules permeate within the mineral structure and are primary constituents of the organic–inorganic interface between the mammillae and the mineral layer (Figures 1 and 2B). Lastly, by applying Stains-all as a staining reagent, the organic and inorganic surfaces of the

composite bioceramic exhibit distinct pink and yellow regions in the mammillae sites and palisade cones, respectively. Given the property of Stains-all to distinguish among sGAGs, the pink and yellow regions correspond to chondroitin or dermatan sulfate and heparan sulfate, respectively. Chondroitin or dermatan sulfate are selectively enriched at the mammillae sites. In the shell surface, however, an enrichment of the respective sGAG in the palisade cones is not observed. On the other hand, the localization of heparan sulfate is higher in the palisade cones, whereas its distribution in the organic membranes is limited to the mammillae surface. The unique localization of different sGAGs reflects the distinct roles of anionic proteoglycans and polysaccharides in the structural reinforcement of the bioceramic, as well as in regulation of mineral growth.
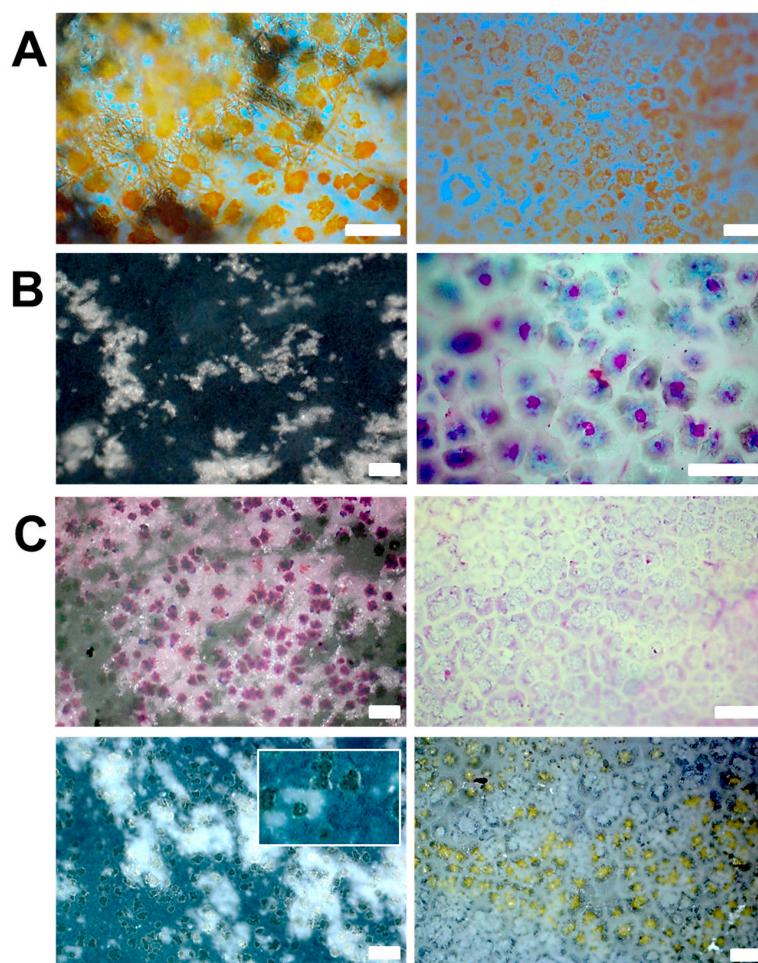


**Figure 2.** Representative images of outer egg membrane (**left** panel) and inner shell (**right** panel) surfaces stained using (**A**) Congo red, (**B**) 1,9-dimethyl-methylene blue (DMMB) and (**C**) Stains-all. Scale bars represent 50 μm (**left** panel) and 100 μm (**right** panel).

An important aspect of the structural integration involving organic and inorganic elements during shell development is the hydrogel-like nature of membrane-associated macromolecules. An organic matrix constituted by diverse macromolecules is likely to exhibit gelation properties in relation to mineralization [12]. Previous studies have shown that the degree of porosity presented by gels regulates mineral structure and form. For instance, the nucleation of mineral particles can either incorporate or exclude the gel structure as exemplified by mineralization in the presence of agarose beads with different degrees of cross-linking [9]. In relation, microscopic observations of the swelling of ethanol-dehydrated mammillae sites indicate changes in light transmittance and, hence, reveal the hydrogel-like properties of membrane-associated macromolecular assemblies (Figure 3A,B;

Supplementary Video). Certain synthetic gels, such as PVA, also exhibit a similar change in light transmittance in relation to conditions of hydration [50]. Based on these observations, as well as the results of calcination and staining experiments, the egg shell scaffold exhibits a chemically-, as well as physically-patterned architecture. The mammillae-bound biomacromolecules and their phase behavior as hydrogels can lead to a distribution of organic macromolecules within a certain extent of the mineral layer (Figure 3C). Thus, the biomineral-bound macromolecules appear to serve multiple purposes involving (i) regulation of mineral nucleation and growth and (ii) incorporation of the mineral phase to generate robust interfaces within the composite structure. To gain a better mechanistic understanding of the biomineralization process, we further investigate in vitro mineralization of the egg shell membrane under the influence of polymeric additives. Since magnesium appears to be a common constituent of egg shells from different species, we apply $Mg^{2+}$ ions as a co-additive to the mineralization reaction.
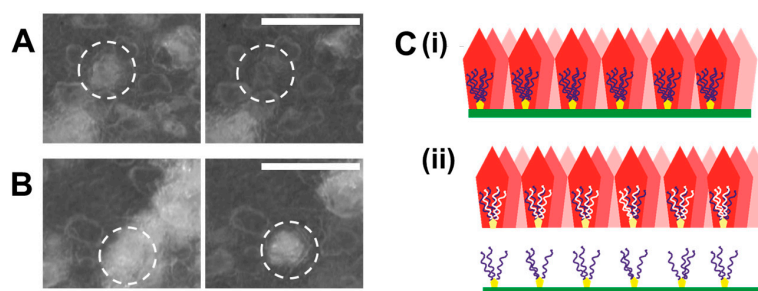


**Figure 3.** (**A**,**B**) Representative images of the hydration process of egg membranes with mammillae sites indicated by dotted circles shown before (**left**) and after (**right**) swelling. Scale bars represent 100 μm. (**C**) Cartoon representation of the egg shell with the mineral (red), collagenous membrane (green), mammillae (yellow) and scaffold-bound hydrogel-like macromolecules (indigo) shown (**i**) before and (**ii**) after decalcification.

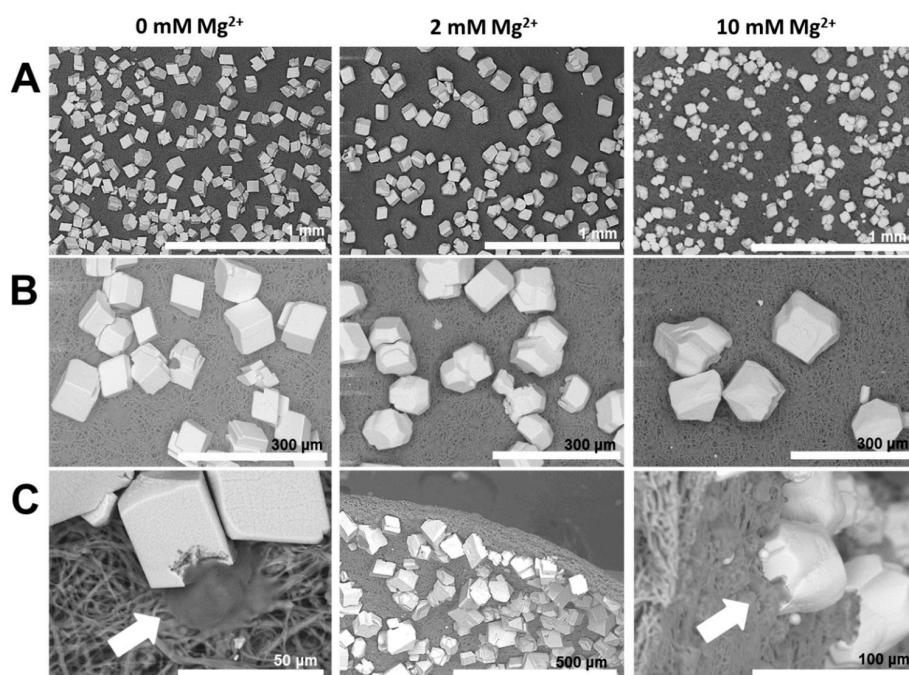## 2.2. Reconstructing the Mineral: Reference Experiments

To investigate the cooperative effects of synthetic polymers and $Mg^{2+}$ ions on mineral retrosynthesis, gas diffusion-based mineralization of decalcified egg shell membranes is performed. In the absence of polymeric additives, diffusion-based mineralization of membranous scaffolds leads to surface growth of crystals, presenting particle morphologies in relation to the $Mg^{2+}$ content (Figure 4). The crystals present shapes ranging from typical calcitic rhombohedra to elongated morphologies. A notable observation is the growth of mineral particles in the proximity of mammillae sites, independent of the co-additive ion content (Figure 4, arrows). The mammillae-associated growth of calcite crystals with a columnar morphology has been reported in the presence of dermatan sulfate and carbonic anhydrase during in vitro calcification [32]. The role of the mammillae as primary nucleation sites during biomineralization is also shown by calcein-stained membranes, suggesting the sequestration and enrichment of $Ca^{2+}$ ions by macromolecules constituting the mammillae (Figure S1). In addition, since crystal formation is limited to the surface of the organic matrix, a suppressed permeation of mineral precursors within the matrix and an inhibitory effect of the collagenous scaffold towards crystal nucleation is indicated (Figure 4C, left).

To investigate the effect of an uncharged polymer as a reference additive on egg membrane-associated $CaCO_3$ crystallization, polyethylene glycol (PEG) is applied during mineralization in the presence of varying $Mg^{2+}$ contents as the co-additive. Although no significant deviation in the polymorph of mineral particles is observed with respect to the reference experiment, certain variations in crystal morphology are evident. In the presence of PEG, calcite crystals grow in association with mammillae (Figure 5C) and tend to exhibit thermodynamically-favored rhombohedral shapes, even at high $Mg^{2+}$ ion contents (10 mM). This suggests the role of PEG in inhibiting $Mg^{2+}$-induced deviations in crystal morphology and in suppressing ion associations that underlay $Mg^{2+}$-induced aragonite formation [51]. For instance, crowded solutions of mineralization additives

lead to significant deviations in mineral nucleation behavior [9,10]. On these lines, high PEG contents can suppress ion-association, inhibit nucleation and also modulate mineral polymorphism, affected by diffusion-limitation and charge screening effects [9,10]. Although lower additive contents are applied in the present study, the effects on nucleation and crystal growth are possibly augmented within confined and crowded regions of the egg shell scaffold.
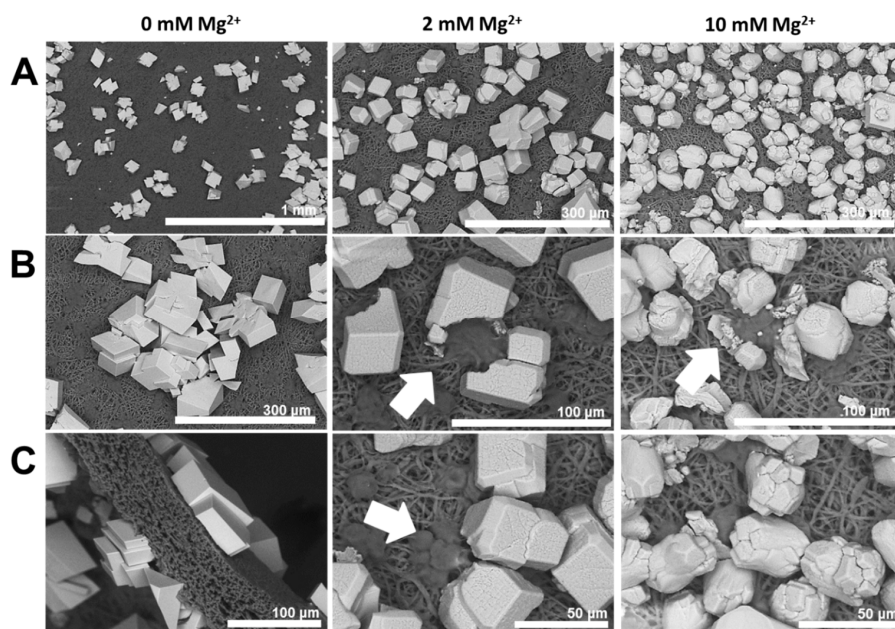


**Figure 4.** Representative SEM images of outer membrane surfaces mineralized in the presence of different $Mg^{2+}$ contents. Arrows indicate mammillae-associated crystals.
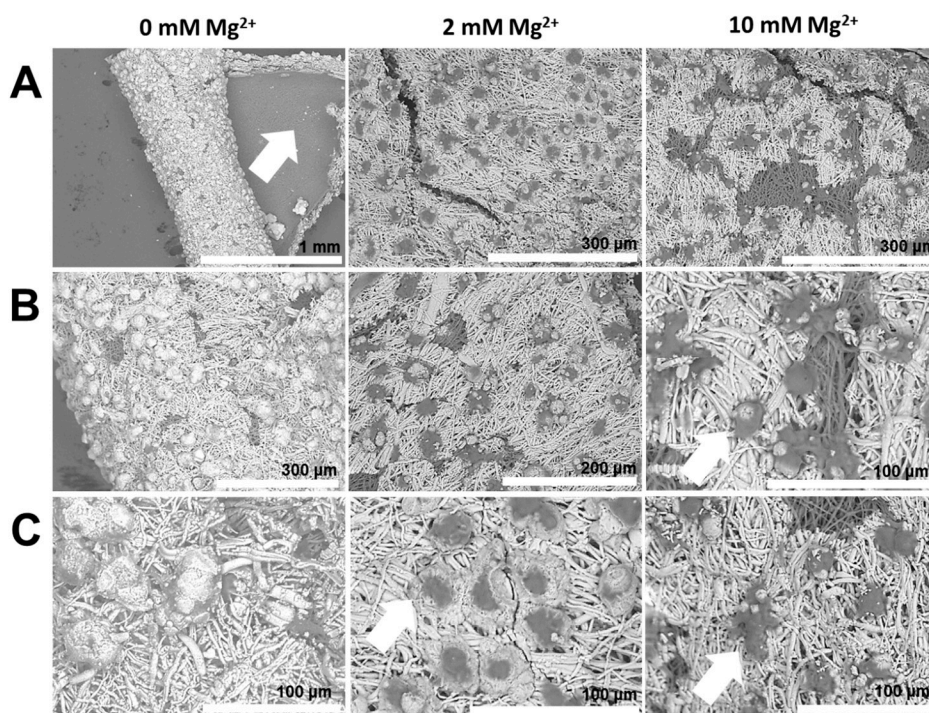


**Figure 5.** Representative SEM images of the outer surfaces of egg shell membranes mineralized in the presence of PEG (50 ppm) and different $Mg^{2+}$ contents. Arrows indicate mammillae-associated crystals.

## 2.3. Reconstructing the Mineral: Poly(acrylic acid)

In order to investigate the effects of charged polymers during scaffold-associated mineralization, poly(acrylic acid) (PAA) of two distinct molar masses, i.e., 5000 g/mol (PAA 5000) and 35,000 g/mol (PAA 35000), is applied as the mineralization additives. Technically applied as a scale inhibitor, PAA is known to interact with soluble pre-nucleation clusters and inhibit the nucleation of mineral particles [52]. PAA interacts with transient mineral precursors and can stabilize amorphous forms of $CaCO_3$ in a potent manner [52–57]. Retro-mineralization of the egg shell scaffold in the presence of PAA provides several insights into the mineralization process (Figure 6). With PAA 5000, the inner and outer side of the membrane (i.e., without and with mammillae respectively) exhibit distinct mineralization patterns. The mammillae-decorated membrane surface is significantly mineralized relative to the inner surface, on account of the nucleation-promoting activity of biomacromolecules presented by mammillae-decorated surfaces (Figure 6A, arrow). In the absence of $Mg^{2+}$ ions, the collagenous membrane, as well as the mammillae sites are mineralized on the outer membrane. This indicates that mineral precursors formed in the presence of PAA are "incompatible" with the nucleation promoting activity of the mammillae. It appears that ion-complexation-based local supersaturation by sulfated macromolecules in the mammillae is suppressed by (i) the competitive association of PAA towards $Ca^{2+}$ ions and (ii) a potent stabilization of mineral precursors in solution by PAA.



**Figure 6.** Representative SEM images of outer surfaces of egg shell membranes mineralized in the presence of poly(acrylic acid) (PAA) 5000 (50 ppm) and different $Mg^{2+}$ contents. Arrows indicate (**A**) membrane curvature post-mineralization and (**B**,**C**) preferential mineralization of collagen fibrils and active exclusion of mammillae from mineral growth.

An interesting observation is the mineralization-induced deformation of the pseudo 2D scaffold, leading to membrane curvature (Figure 6A, left). This feature is not observed in reference experiments and hints towards a mechanism involving the initial association of mineral precursors with the substrate and subsequent phase transition to the crystalline phase. During this process, a selective enrichment and incorporation of the mineral phase on one side of the 2D organic matrix can lead to distinct swelling of the inner and outer surfaces, in turn causing membrane deformation (Figure 7). An analogous example can be drawn from the binding of certain proteins to lipid membranes

involving domain insertion in the membrane, causing lateral expansion and curvature of the membrane bilayer [58]. Similarly at the mesoscale, in the present scenario, curvature of the egg scaffold in the course of mineralization can involve contributions from (i) mineral particles causing expansion of one side of the collagen scaffold and (ii) distinct stiffness presented by the mineral occupied and the bare organic surface of the scaffold (Figure 7). These factors are consistent with the observed direction of curvature, with the mineralized surface being presented outwards. Such processes might play a morphogenetic role during biogenic mineralization. In Nature, during egg development, the shell membranes cover the secreted albumen, and before the shell is mineralized, the developing egg undergoes the process of "plumping" (hydration), i.e., water and salts are pumped into the egg, swelling it and exposing the stretched mammillae surfaces in a manner that determines the egg size and shape [59].
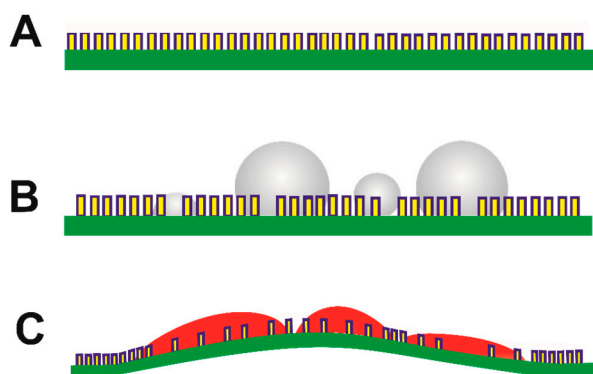


**Figure 7.** Schematic depiction of the putative membrane curvature mechanism involving (**A**,**B**) specific interactions of mammillae-decorated (yellow) collagenous membrane (green) and mineral precursors (grey); (**C**) the enrichment of mineral precursors and phase transformation to crystalline forms (red) induce surface localized swelling of the membrane and subsequent membrane deformation and curvature.

The effects of PAA on egg scaffold re-mineralization are distinct in the presence of different $Mg^{2+}$ ion contents (Figure 6). The collagenous membrane of the egg shell is a known inhibitor of crystal nucleation in the context of egg shell biomineralization [32]. However, in the presence of PAA, crystal growth is favored in the proximity of the collagenous membrane, whereas the mammillae are relatively less mineralized (Figure 6B,C, arrows). This effect becomes significant with increasing levels of $Mg^{2+}$ ions. In the context of the established roles of additives with carboxylate, phosphate or sulfate residues in biomineralization systems [3,60], it emerges that synergetic relations with co-additive species, including ions, are crucial for the selective emergence of the biomineral structure and properties. Furthermore, previous studies on biomimetic mineralization of collagen via polymer-stabilized PILPs demonstrate the role of liquid mineral precursors in attaining biomimetic mineralization in confined spaces analogues to the natural scenario [61,62]. Here, we show that the amorphous phases cooperatively stabilized by PAA and $Mg^{2+}$ ions preferentially mineralize collagen, as indicated by relatively suppressed mineral growth at mammillae sites (Figure 6B,C, arrows). As this trend is significant in the presence of $Mg^{2+}$ ions, the role of co-additive ion species in tuning the interactions between the mineral precursors and the biomineral matrix is demonstrated. In a previous study, $Mg^{2+}$ has been shown to tune the wettability of liquid-like mineral precursors depending on the functionalization of bioinspired substrates [45]. Therefore, even in the context of a biogenic scaffold, the association between mineral precursors and the organic matrix is determined by the $Mg^{2+}$ content (Figure 6). Possible factors underlying $Mg^{2+}$ ions favoring collagen mineralization include (i) the role of ion species in tuning the transient organic–inorganic interface (e.g., via electrostatic repulsion or charge screening effects, given the topological enrichment of sulfated biomacromolecules in the scaffold) and

(ii) its role as a potent nucleation inhibitor, as well as a suppressor of ion-association in combination with PAA [43], which can lead to a low size regime of mineral precursors better compatible with the dimensions of confined zones within the collagen super-assembly.

Application of a high molar mass PAA (PAA 35000) during ex situ mineralization of the egg membrane provides certain similar trends as PAA 5000 (Figure 8). For instance, in the presence of $Mg^{2+}$ ions, mineralization of collagen fibrils is clearly favored (Figure 8, arrows). However, a unique feature observed in the presence of PAA 35000 is the formation of two-dimensional crystal structures exhibiting porosities akin to a Swiss-cheese texture (Figure 9A,B). A comparable structure has been described earlier for monocrystalline mineral products produced using substrates with micropatterned chemical functionalities [63]. Therefore, the morphology derived during egg membrane-assisted mineralization is possibly related to the distinct localization of anionic biomacromolecules, mammillae distribution, as well as the void spaces of the collagen mesh. An additional contributing factor might be the release of additive species, such as PAA 35000 and $Mg^{2+}$ ions from the mineral precursor during phase transformation towards crystalline forms. This process likely involves a microphase separation involving the transient enrichment and solubilization of additive species. In contrast to the monocrystalline sheets formed on micropatterned substrates as described earlier [63], quantitative polarization mapping of individual mineral sheets formed on the egg shell membrane shows distinct crystallographic domains constituting each porous sheet (Figure 9B). This reflects the contribution of multiple phase transition events in the formation of individual mineral superstructures. Since this feature specifically emerges in the presence of PAA of higher molar mass, the relation between additive molar mass and the properties of intermediate amorphous phases, such as stability and size distribution, appears critical for the emergence of superstructures. Previous studies indicate that the molar mass of PAA is an important determinant of the liquid- or gel-like form of amorphous intermediates [55,56], suggesting corresponding effects on the shape and structure of subsequently-formed mineral products.
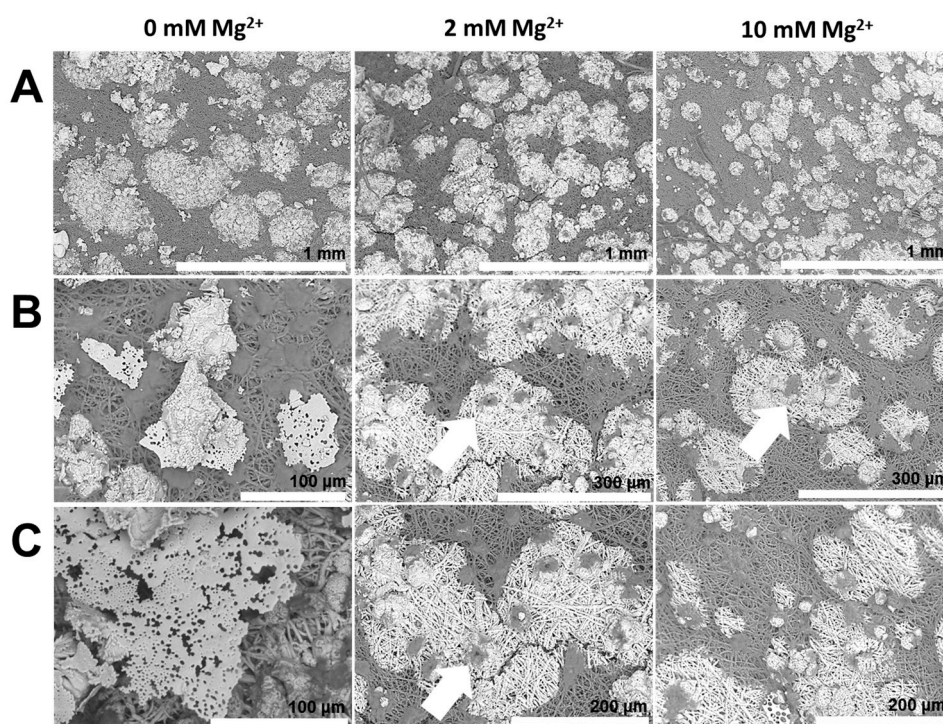


**Figure 8.** Representative SEM images of outer surfaces of egg shell membranes mineralized in the presence of PAA 35000 (50 ppm) and different $Mg^{2+}$ contents. Arrows indicate the exclusion of mammillae from crystallization.
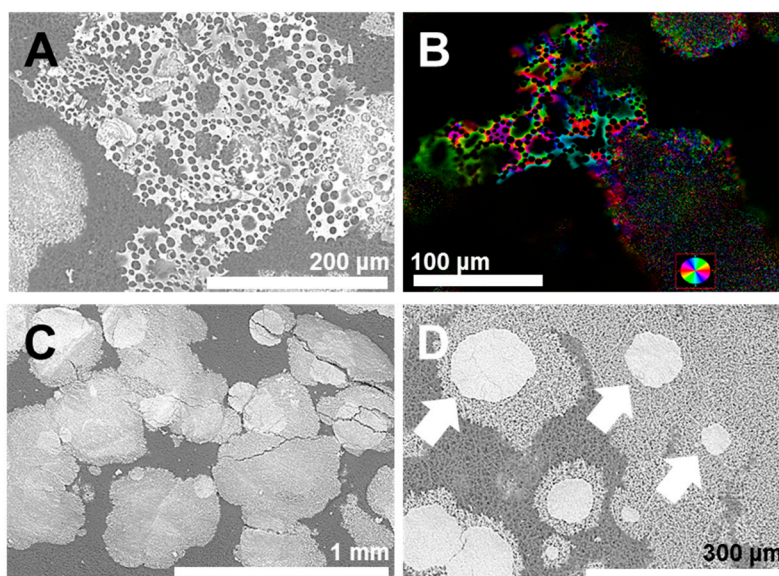
**Figure 9.** Representative SEM images of mineralized (**A**) outer and (**C**,**D**) inner surfaces of egg shell membranes in the presence of PAA 35000 (50 ppm); (**B**) crystallographic domains from quantitative polarization mapping (Abrio©, CRi, Woburn, MA, USA) of the mineral structure corresponding to (**A**).

An interesting feature of phase transitions associated with the mineral precursor is identified for mineralization on the inner membrane surface, i.e., devoid of mammillae (Figure 9C,D). Mineral structures suggestive of multiple wetting and phase transition events indicate that the "secondary wetting" by the PILP droplets is favored at mineralized surfaces relative to bare collagen surfaces. Therefore, the preferential association of mineral precursors with sites on the biomineral matrix is due to the distinct interfaces presented by collagen-rich surfaces with and without mineral growth. Under the applied experimental conditions, the initially-formed calcitic surfaces being hydrophilic and less charged in comparison to the organic surface lead to the preferential adsorption of PAA-stabilized mineral precursors. In addition, the flat surface of mineral products formed after secondary wetting is indicative of almost complete wetting (Figure 9D) and suggests that complete wetting by the mineral precursor precedes phase transition. Thus, the induction of phase transition by either the organic matrix or crystalline particles can lead to distinct consequences for mineralization pathways, as depicted in Figure 10.

In view of mineralized structures formed via polymer stabilized gel- or liquid-like mineral precursors and heterogeneous substrates, the role of surface properties in relation to wettability needs to be considered. Since the size distribution of the mineral precursors appears sufficiently large relative to the roughness of the membrane (Figure 9C,D), one might consider classical models that describe wetting of textured surfaces (Figure 11). According to the Cassie–Baxter model, for wetting of heterogeneous surfaces (such as the collagen substrate), the apparent contact angle is described as:

$$\cos\theta^* = rf\cos\theta_Y + f - 1$$

where $r$ is the surface roughness, $f$ is the fraction of substrate surface area wetted by the liquid and $\cos\theta_Y$ is the contact angle for a flat surface. In the case of mineral precursors wetting the collagenous substrate, water initially occupying the gaps of the fibrils (i.e., high surface roughness) may result in a larger contact angle presented by the transient mineral phase, resulting in a temporary Cassie–Baxter state. Subsequently, due to the gradual displacement of solvent molecules by the precursor, complete wetting behavior results (i.e., Wenzel state). Considering mineralization via liquid- or gel-like precursors [56,64], the presence of droplet-like and sheet-like structures is indicative of a Cassie–Baxter or Wenzel state, respectively (Figure 11). During mineralization experiments using PAA

5000 and 35000 as polymeric additives, it appears that the transition from the Cassie–Baxter to the Wenzel state is rapid, as indicated by close to complete wetting of the substrate, finally resulting in flat mineral textures (Figure 9C,D). As shown for other systems, the energy barriers associated with wetting transitions are affected by multiple factors, such as interfacial energy and Laplace pressure [65]. These parameters need to be addressed in the case of fluidic mineral precursors and organic surfaces. Solely considering the rough texture presented by the collagen network, a low general wettability of the organic matrix is expected. However, the final structure of the mineral products suggesting complete wetting, the contribution of distinct chemical environments modulating polar and van der Waals interphasic interactions, as well as the nature of the transient mineral phase require elucidation.
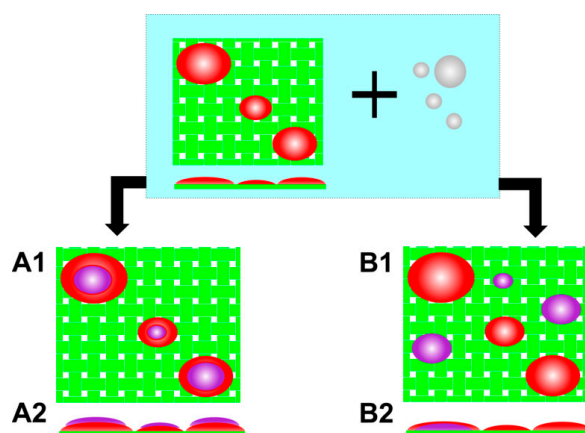


**Figure 10.** Schematic models for the emergence of distinct mineral superstructures favored via (**A**) mineral-induced or (**B**) organic matrix-induced preferential crystallization of mineral precursors. Crystallization of the amorphous phase (grey) in association with the collagenous matrix (green) or pre-formed crystalline particles (red) lead to distinct mineralization patterns involving subsequent mineral particles (violet). The top-view and side-view are represented by the suffixes 1 and 2, respectively.
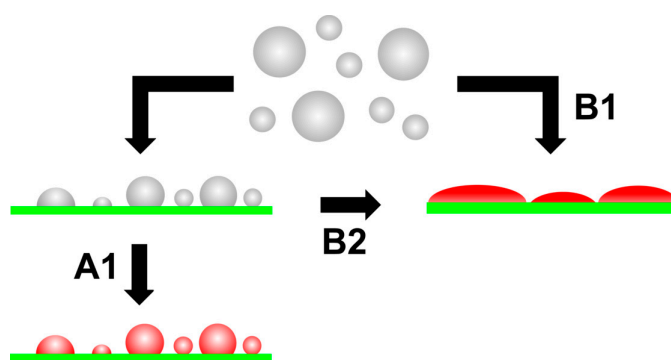


**Figure 11.** Schematic depiction of interactions between mineral precursors (grey) and the organic matrix (green), involving the subsequent formation of crystalline products (red). (**A1**) Rapid phase transformation of polymer-induced liquid precursor (PILP) droplets that partially wet the organic surface leads to droplet-shaped mineral particles. Organic–inorganic interactions favoring a Wenzel state (i.e., complete wetting) lead to sheet-like structures via (**B1**) a matrix-induced crystallization of a PILP phase involving rapid, complete wetting or (**B2**) an intermediate Cassie–Baxter state involving phase transformations on a timescale significantly slower relative to the dynamics of the PILP phase.

*2.4. Reconstructing the Mineral: Poly(aspartic acid)*

Given the anionic nature of poly(aspartic acid) (PASP, 2000–3000 g/mol) and its role in stabilization of amorphous precursors, morphologies similar to that of PAA as the mineralization additive might

be expected. However, at the applied polymer contents (50 ppm) and in the absence of $Mg^{2+}$ ions, calcitic rhombohedra are observed in the proximity of mammillae sites (Figure 12, arrows), similar to the reference and PEG-containing experiments. On the outer membrane, mineral particles in association with the mammillae appear rounded and irregular, as well as exhibit a broad size distribution, with increasing contents of $Mg^{2+}$ ions (Figure 12). Such structures are reminiscent of a Cassie–Baxter state and suggest a PILP phase with enhanced stability and cohesivity. In comparison to shell membranes mineralized in the presence of PAA, the co-association of mineral particles with mammillae for PASP and PEG as additives shows that the anionic properties of soluble additives are not the sole determinants for crystal nucleation. Properties such as additive conformation and molar mass, as well as inter-/intra-molecular interactions tune nucleation events. This is also indicated by assaying saccharide additives using a potentiometric titration methodology [66]. Since mineral precursors formed in the presence of PASP crystallize specifically in proximity of mammillae sites (Figure 12), the interactions of mammillae constituents appear to destabilize the transient mineral phase, inducing crystallization. This suggests cooperative interactions between sulfated proteoglycans and transiently-stabilized mineral precursors in spatially directing mineral nucleation. Supporting evidence comes from the function of a keratan sulfate proteoglycan isolated from the membrane in promoting the nucleation of less soluble phases (i.e., crystalline) of $CaCO_3$ under in vitro conditions [30]. In the presence of PASP, an interesting feature is the prevalence of mineral morphologies on the outer membrane, which are suggestive of a PILP phase, specifically in the presence of $Mg^{2+}$ ions. This agrees with mineralization studies that utilize peptide additives, wherein the co-presence of $Mg^{2+}$ ions promotes the formation of liquid-like precursors of $CaCO_3$ [67].
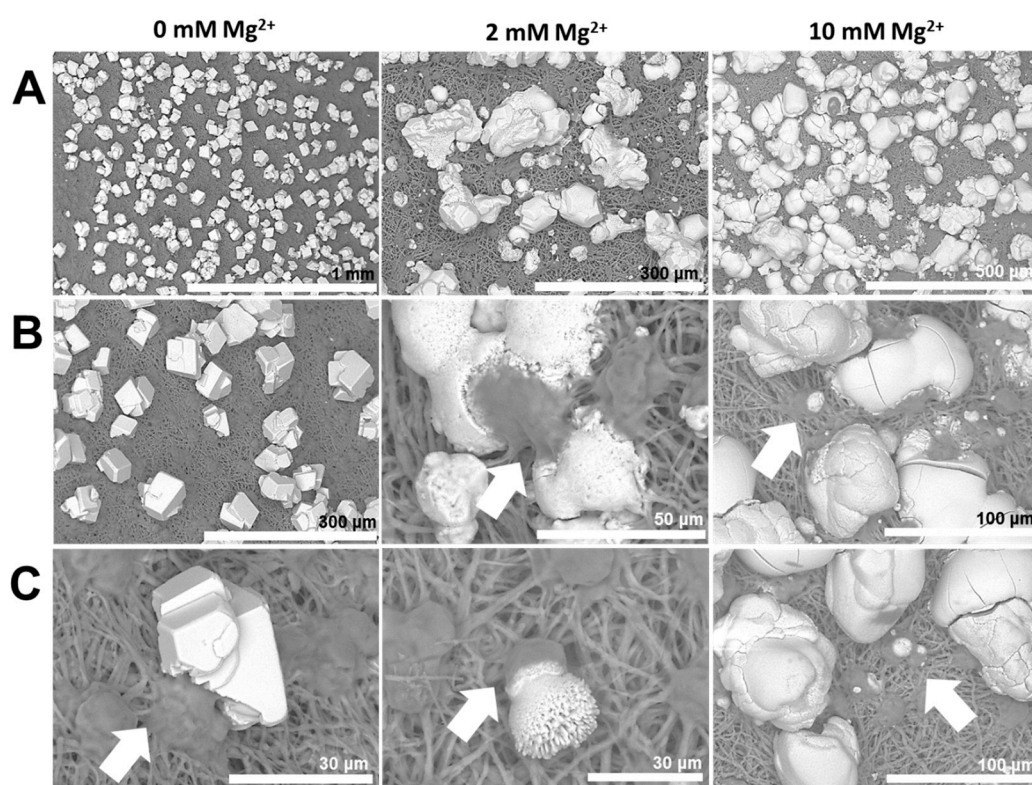


**Figure 12.** Representative SEM images of the outer surfaces of egg shell membranes mineralized in the presence of poly(aspartic acid) (50 ppm) and different $Mg^{2+}$ contents. Arrows indicate mammillae-associated crystals.

As shown for PAA as a mineralization additive, in the presence of PASP, distinct interactions of the mineral precursors occur with the inner and outer surfaces of the heterogeneous scaffold. Observations

of the inner egg membrane post-mineralization exhibit distinct mineral morphologies in relation to the $Mg^{2+}$ content (Figure 13). In the absence of $Mg^{2+}$ ions, mineral precursors mostly exhibit spherical shapes with smooth surfaces formed due to partial wetting, as well as sheets formed due to complete wetting of the collagenous substrate (Figure 13, left). This hints towards a rapid transition from the Cassie–Baxter to Wenzel state. However, with $Mg^{2+}$ ions (10 mM), an increased cohesivity of the liquid precursor is indicated by the absence of mineral sheets and the prevalence of spherical particles (Figure 13, right). This hints towards the stabilization of a Cassie–Baxter state and modulation of cohesivity by $Mg^{2+}$ ions. A distinct feature of such particles is a porous texture, which reflects the role of demixing mechanisms involving the sequestration of a highly soluble (polymer-rich) phase.
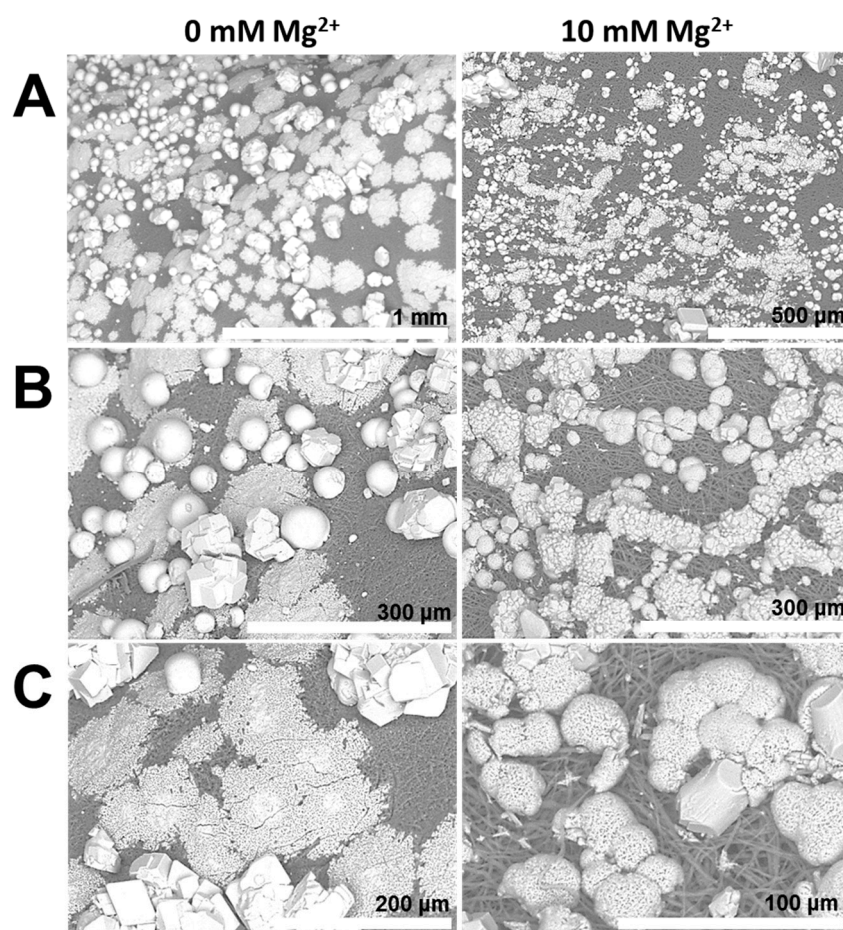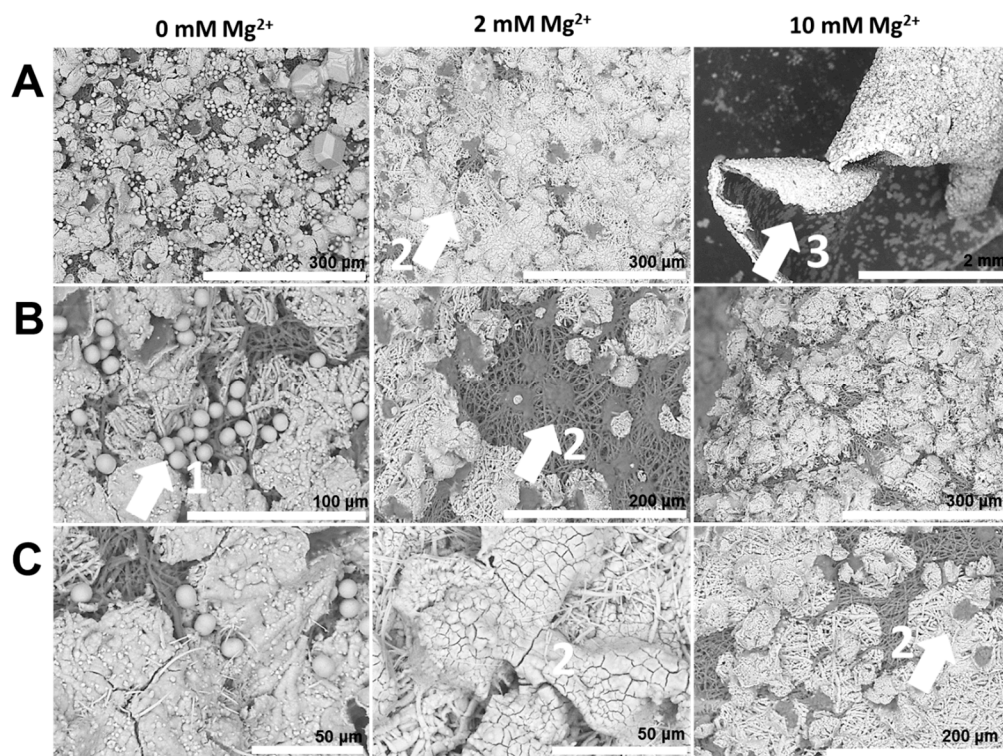


**Figure 13.** Representative SEM images of mineralized inner surfaces of egg shell membranes in the presence of poly(aspartic acid) (PASP) with (**right** panel) and without (**left** panel) $Mg^{2+}$ ions.

### 2.5. Reconstructing the Mineral: Poly(4-styrenesulfonic acid-co-maleic acid)

The role of PSS-*co*-MA in controlling the superstructure of mineral products is well demonstrated. Mediated by non-classical crystallization processes, a systematic control over the size, structure and morphology of particles is achieved by applying PSS-*co*-MA during $CaCO_3$ growth [68,69]. Given the functions of sulfated macromolecules in egg shell mineralization [48], PSS-*co*-MA (molar mass 20,000 g/mol) is an interesting synthetic counterpart and is evaluated as an additive during retro-mineralization of the egg biomineral. In the absence of $Mg^{2+}$ ions, an extensive surface mineralization of the mammillae-occupied outer membrane is evident (Figure 14). The spatial control over mineral growth is minimal, reflected by mineralization at the mammillae sites, as well as in proximity to the collagen fibers. In this regard, the effects of PSS-*co*-MA and PAA on crystal nucleation are similar and contrast the biomimetic mammillae-associated mineral nucleation observed in the

reference, as well as PEG- or PASP-containing experiments. In addition, in the presence of PSS-*co*-MA and $Mg^{2+}$ ions, mineralization induces a significant curvature of the organic membrane, on account of a higher mineralization propensity exhibited by the mammillae-covered surface (Figure 14A, right). This mineralization outcome is also noted in the presence of PAA and reflects a mechanical actuation behavior because of anisotropic mineralization propensities (Figure 7).



**Figure 14.** Representative SEM images of outer surfaces of shell membranes mineralized in the presence of PSS-*co*-MA (50 ppm) and different $Mg^{2+}$ contents. Arrows indicate (1) spherical particles formed in the absence of $Mg^{2+}$ ions, (2) a higher degree of mineralization of collagen fibrils relative to mammillae and (3) distinct mineralization on inner and outer membrane surfaces.

An interesting observation is the presence of spherical particles, the remnant of a liquid-like $CaCO_3$ intermediate, in the absence of $Mg^{2+}$ ions (Figure 14). With increasing contents of $Mg^{2+}$ ions, the abundance of the spherical particles decreases; however, the extensive mineralization of the biogenic scaffold is retained. Therefore, in the presence of PSS-*co*-MA, $Mg^{2+}$ ions appear to decrease the transient stability of a liquid- or gel-like mineral precursor. With increasing $Mg^{2+}$ contents, the mammillae sites are preferentially excluded from mineral nucleation, and collagen fibers are the preferred substrate for mineralization. Possible reasons suggested for this trend are: (i) $Mg^{2+}$ ions decrease the stability of the intermediate mineral phases and lead to a rapid and relatively less controlled crystallization processes and (ii) $Mg^{2+}$ ions modulate interfacial interactions between the transient mineral phase and the biomineral scaffold.

## 2.6. Polymorph Selection during Scaffold-Assisted Mineralization

The emergence of distinct mineral polymorphs is analyzed by performing FTIR spectroscopy of the membranes mineralized ex situ (Figure S2). Reference experiments that lack polymeric additives produce calcite as the predominant mineral phase, independent of $Mg^{2+}$ content. Since mineralizing solutions with a relatively high $Mg^{2+}$ content (1:1 $Ca^{2+}$:$Mg^{2+}$ ratio) produce a calcite-rich phase associated with the egg membrane, the contribution of the biogenic scaffold in polymorph selection is significant. An alternate explanation is the binding of $Mg^{2+}$ ions by anionic constituents of the egg

matrix; however, for the reason that calcite is nucleated even at 10 mM of $Mg^{2+}$ ions, the contribution of this factor appears minimal. A similar trend is identified in the presence of PEG as the mineralization additive. Therefore, the capacity of the egg shell scaffold towards inducing calcite formation, even surpassing the effects of $Mg^{2+}$-induced aragonite formation, is remarkable.

Polymeric additives have distinct effects on the polymorph formed during biomineral retrosynthesis. In the presence of PAA 5000, calcite is the predominant mineral phase irrespective of the $Mg^{2+}$ content. However, with a higher molar mass PAA 35000, distinct mineral phases are stabilized as determined by $Mg^{2+}$ ion content. In the absence of $Mg^{2+}$ ions, ACC is the major mineral phase, as indicated by a peak at 863 cm$^{-1}$ ($v_2$). With increasing $Mg^{2+}$ contents, this peak shifts towards 854 cm$^{-1}$ ($v_2$), indicating aragonite formation. Thus, the molar mass of PAA as a mineralization additive significantly affects Oswald ripening behavior and polymorph selection of the mineral phase. With PASP as the additive, calcite is formed as the major product after mineral retrosynthesis, independent of the $Mg^{2+}$ content. On the other hand, PSS-*co*-MA leads to calcite or aragonite formation in the absence or presence of $Mg^{2+}$ ions, respectively. Therefore, the capacity of $Mg^{2+}$ ions to induce aragonite formation is either suppressed or relatively unaffected in the presence of PASP or PSS-*co*-MA, respectively. In this regard, in complex biological environments that consist of multiple ingredients, the synergistic interactions between additives species significantly affect mineralization outcomes. In addition, the concentration of $Mg^{2+}$ ions as a co-additive species significantly affects the influence of organic additives on nucleation and crystallization processes.

## 3. Materials and Methods

### 3.1. Materials

Eggs from commercial White Leghorn laying hens are used. The internal egg contents are discarded through a perforation, and the shells are washed several times with de-ionized water. The egg is filled with 5% acetic acid, incubated for 30 min, and the separated outer shell and inner membranes are used for subsequent experiments. Mineralization experiments utilize calcium chloride ($CaCl_2$, 1 M, Sigma, St Louis, MO, USA) and ammonium carbonate (Merck, Kenilworth, NJ, USA). Mineralization additives include magnesium chloride ($MgCl_2 \cdot 6H_2O$, Merck), polyethylene glycol of molar mass 5000 g/mol (PEG), poly(acrylic acid) of molar masses 5000 g/mol (PAA 5000) and 35,000 g/mol (PAA 35000), poly(aspartic acid) (Baypure DS100, LANXESS Corporation, Pittsburgh, PA, USA) of molar mass in the range of 2000 to 3000 g/mol (PASP) and poly(4-styrenesulfonic acid-*co*-maleic acid) of molar mass 20,000 g/mol (PSS-*co*-MA). All solutions are prepared using Milli-Q water (Millipore Corporation, Milford, MA, USA).

### 3.2. Staining and Swelling Studies

Surfaces of the shell and membrane materials are stained using Stains-all, Congo-red and 1,9-dimethyl-methylene blue (DMMB). Stains-all staining solution is prepared by diluting a stock solution (10×, 0.1% (*w/v*) in formamide) in Tris (20 mM, pH 8) containing 25% (*v/v*) isopropanol. Staining with Congo red is done using a solution containing 0.01% (*w/v*) dye in Tris buffer (0.5 M, pH 8.0). DMMB solution contains 0.01% (*w/v*) stain prepared in acetic acid (0.1 M) containing sodium chloride (0.1 M). After incubating samples in the respective staining solutions, the samples are rinsed to remove excess stain and visualized using a Zeiss Axio Imager M2m optical microscope (Wetzlar, Germany). Optical observations of membrane swelling behavior are performed by initial dehydration in absolute ethanol, followed by swelling by the addition of water.

### 3.3. Gas Diffusion-Based Mineralization

Egg shell membranes are decalcified by extensive washes using 5% acetic acid, followed by several washes with water to remove any traces of acid. Using sterile 12-well, flat bottom plates (Corning®, Corning, NY, USA), a membrane piece is submerged in calcium chloride (10 mM) solution containing

either 0, 2 or 10 mM magnesium chloride. The plate is exposed to $CO_2$ generated by the decomposition of ammonium carbonate in a sealed desiccator. After incubation for 3 days, the membranes are washed with absolute ethanol to remove weakly-attached crystals. Mineralized scaffolds are analyzed using (i) a desktop Scanning Electron Microscopy (SEM) (Hitachi TM-3000, Tokyo, Japan) and (ii) a Zeiss Axio Imager M2m optical microscope with polarizers and accessories for quantitative birefringence imaging.

## 4. Conclusions

Composite biominerals engineered by Nature exhibit remarkable formation routes and material properties. Of recent developments in the field of biomineralization, the nature of inorganic precursors, such as ion-clusters and amorphous phases, are shown crucial for mineral nucleation and growth [70,71]. For instance, in the presence of certain charged additives, stabilized amorphous phases exhibit fluid- or gel-like properties, suggested in enabling homeostatic mineralization (that involves an elegant integration with the organic matrix at different length scales). Of relevance is the occurrence of biogenic mineralization in non-ideal confined and crowded spaces, which significantly alters the pathways of nucleation and crystallization [10]. Thus, the in situ dynamics of the inorganic–organic interface from nascent to final stages of mineral formation must be addressed for a better understanding of biomineralization.

In the present study, we show that sulfated proteoglycans present distinct shell- and membrane-associated spatial distributions in the composite egg bioceramic. By applying the strategy of demineralization that yields intact organic scaffolds [72], we provide insights into biomineralization processes, as well as inspire soft materials for biomimetic mineralization. For instance, identified by using Stains-all reagent, heparan sulfate and chondroitin or dermatan sulfate are selectively enriched within the shell structure and at the membrane-bound mammillae sites, respectively. The patterns of localization reflect that the phase partitioning of certain sGAGs towards the growing mineral is favorable, leading to a selective enrichment of biomacromolecules within the mineral. Although this process has also been suggested in the emergence of diverse hierarchical structures of biominerals [71], in the case of the egg shell, the infiltration of organic additives within the mineral provides a robust interface between the organic substrate and the mineral layers. Supporting evidence comes from the hydrogel nature of egg membrane-associated macromolecules. Since gel porosity determines the selective inclusion or exclusion of mineral particles [9], the physical nature of additives as supramolecular assemblies (such as gels) is critical for the structural reinforcement of certain biominerals. In this manner, the distinct localization of additives and the hydrogel nature of additive macromolecules provide respective chemical and physical checkpoints for biomineralization. Thus, the egg membrane represents a micropatterned quasi-two-dimensional substrate designed by Nature in order to achieve a sophisticated control over mineral growth.

The present study also elucidates the emergence of mineral form and structure during the retrosynthesis of the egg shell under the combined influence of synthetic polymers and $Mg^{2+}$ ions. Important aspects identified during retro-mineralization of the biogenic scaffold are:

1. The formation of aragonite, which is typically induced by $Mg^{2+}$ ions, is suppressed by the organic matrix of the egg shell. This hints that the biochemical environment presented by the egg membrane actively promotes calcite formation. Applying PAA 35000 during mineralization, the polymorph selectivity towards calcite is rendered ineffective possibly via charge screening and competitive ion-binding by additive molecules. Therefore, biomineral scaffolds and soluble additives operate synergistically during mineral polymorph selection.
2. Mineralization additives with similar anionic groups can produce diverse mineral products in terms of shape, size, structure, as well as crystallographic orientation, due to the distinct molecular aspects of additives, such as conformation and chain-backbone chemistry. For instance, PASP leads to mammillae-associated nucleation of $CaCO_3$ crystals. However, PAA 5000 leads to profuse surface mineralization, irrespective of mammillae distribution. Therefore, properties of additives, such as conformation and self-association, emerge as critical factors regulating mineralization.

3.　The molar mass of a mineralization additive profoundly affects mineral structure. For instance, unlike PAA 5000, PAA 35000 leads to microporous sheets formed via multiple nucleation events, in association with the egg membrane.

4.　Certain anionic additives lead to deformation and curvature of the egg organic matrix in the course of mineral growth. Phase transformation of attached mineral precursors induces surface-localized deformation of the membrane and subsequent membrane curvature. Similar mechanisms may operate during biogenic mineralization, determining the morphological aspects at larger length scales. To the best of our knowledge, this is the first report of mineralization-induced mechanical actuation.

5.　Primary and secondary nucleation are distinct due to the surface properties of bare and mineralized organic surfaces. In case of the collagen membrane, secondary wetting by liquid-like mineral precursors preferentially occurs on mineralized surfaces relative to the bare collagenous membrane. Underlying factors include the inhibitory activity of collagen towards mineral nucleation, distinct properties of organic and mineral surfaces and the induction of phase transformation by initially-formed crystalline particles. Therefore, in this context, the primary nucleation event is of utmost importance and lays the foundation of subsequent nucleation events encompassing mineral maturation.

6.　Properties of the mineral precursor phase, as well as subsequently-formed mineral products are determined by the nature of additive and co-additive species. For instance, on the inner surface of the egg membrane, in the presence of PASP, mineral particles with smooth surfaces suggestive of PILP droplets are formed. However, with the addition of $Mg^{2+}$ ions, the particle surfaces are significantly coarse, suggesting a distinct mineralization process.

Given the structure-property relationships and rapid growth of the egg shell composite, the associated growth mechanisms have attracted considerable research attention. In this study, we show that the chemical and physical heterogeneity of the egg shell matrix serves important functional purposes during biomineralization. Organic–inorganic interactions prevalent during mineral formation are tuned by macromolecules, as well as dissolved ion species. Deciphering the true nature of biochemical environments and organic–inorganic interactions sustaining biomineralization will certainly aid the development of bioinspired composite materials.

**Author Contributions:** Experimental tasks and preliminary manuscript draft were realized by Ashit Rao. Project conception and supervision as well as detailed editing of manuscript were performed by José L. Arias and Helmut Cölfen.

**Conflicts of Interest:** The authors declare no conflict of interest.

## References

1.　Weiner, S.; Addadi, L. Crystallization pathways in biomineralization. *Annu. Rev. Mater. Res.* **2011**, *41*, 21–40. [CrossRef]

2.　Lowenstam, H.A.; Weiner, S. *On Biomineralization*; Oxford University Press on Demand: Oxford, UK, 1989.

3.　Mann, S. *Biomineralization: Principles and Concepts in Bioinorganic Materials Chemistry*; Oxford University Press on Demand: Oxford, UK, 2001; Volume 5.

4.　Mao, L.-B.; Gao, H.-L.; Yao, H.-B.; Liu, L.; Cölfen, H.; Liu, G.; Chen, S.-M.; Li, S.-K.; Yan, Y.-X.; Liu, Y.-Y. Synthetic nacre by predesigned matrix-directed mineralization. *Science* **2016**, *354*, 107–110. [CrossRef] [PubMed]

5.  Lee, K.; Wagermaier, W.; Masic, A.; Kommareddy, K.P.; Bennet, M.; Manjubala, I.; Lee, S.-W.; Park, S.B.; Cölfen, H.; Fratzl, P. Self-assembly of amorphous calcium carbonate microlens arrays. *Nat. Commun.* **2012**, *3*, 725. [CrossRef] [PubMed]

6.  Heuer, A.; Fink, D.; Laraia, V.; Arias, J.; Calvert, P.; Kendall, K.; Messing, G.; Blackwell, J.; Rieke, P.; Thompson, D. Innovative materials processing strategies. *Science* **1992**, *255*, 1098–1105. [CrossRef] [PubMed]

7.  Rao, A.; Cölfen, H. Morphology control and molecular templates in biomineralization. In *Biomineralization and Biomaterials: Fundamentals and Applications*; Woodhead Publishing: Cambridge, UK, 2015; pp. 51–93.

8.  Hovden, R.; Wolf, S.E.; Holtz, M.E.; Marin, F.; Muller, D.A.; Estroff, L.A. Nanoscale assembly processes revealed in the nacroprismatic transition zone of pinna nobilis mollusc shells. *Nat. Commun.* **2015**, *6*, 10097. [CrossRef] [PubMed]

9.  Rao, A.; Cölfen, H. On the biophysical regulation of mineral growth: Standing out from the crowd. *J. Struct. Biol.* **2016**, *196*, 232–243. [CrossRef] [PubMed]

10. Rao, A.; Cölfen, H. Mineralization and non-ideality: On nature's foundry. *Biophys. Rev.* **2016**, *8*, 309–329. [CrossRef]

11. Evans, J.S. "Liquid-like" biomineralization protein assemblies: A key to the regulation of non-classical nucleation. *CrystEngComm* **2013**, *15*, 8388–8394. [CrossRef]

12. Rao, A.; Vásquez-Quitral, P.; Fernández, M.S.; Berg, J.K.; Sánchez, M.; Drechsler, M.; Neira-Carrillo, A.; Arias, J.L.; Gebauer, D.; Colfen, H. Ph-dependent schemes of calcium carbonate formation in the presence of alginates. *Cryst. Growth Des.* **2016**, *16*, 1349–1359. [CrossRef]

13. Rao, A.; Seto, J.; Berg, J.K.; Kreft, S.G.; Scheffner, M.; Cölfen, H. Roles of larval sea urchin spicule SM50 domains in organic matrix self-assembly and calcium carbonate mineralization. *J. Struct. Biol.* **2013**, *183*, 205–215. [CrossRef] [PubMed]

14. Du, C.; Falini, G.; Fermani, S.; Abbott, C.; Moradian-Oldak, J. Supramolecular assembly of amelogenin nanospheres into birefringent microribbons. *Science* **2005**, *307*, 1450–1454. [CrossRef] [PubMed]

15. Jain, G.; Pendola, M.; Rao, A.; Cölfen, H.; Evans, J.S. A model sea urchin spicule matrix protein self-associates to form mineral-modifying protein hydrogels. *Biochemistry* **2016**, *55*, 4410–4421. [CrossRef] [PubMed]

16. Bera, T.; Ramachandrarao, P. A chicken's egg as a reaction vessel to explore biomineralization. *J. Bionic Eng.* **2007**, *4*, 133–141. [CrossRef]

17. Arias, J.L.; Arias, J.I.; Fernandez, M.S. Avian eggshell as a template for biomimetic synthesis of new materials. In *Handbook of Biomineralization: Biomimetic and Bioinspired Chemistry*; Wiley-VCH Verlag, GmBH & Co: Weinheim, Germany, 2007; Volume 2.

18. Fernandez, M.S.; Araya, M.; Arias, J.L. Eggshells are shaped by a precise spatio-temporal arrangement of sequentially deposited macromolecules. *Matrix Biol.* **1997**, *16*, 13–20. [CrossRef]

19. Carrino, D.A.; Dennis, J.E.; Wu, T.-M.; Arias, J.L.; Fernandez, M.S.; Rodriguez, J.P.; Fink, D.J.; Heuer, A.H.; Caplan, A.I. The avian eggshell extracellular matrix as a model for biomineralization. *Connect. Tissue Res.* **1996**, *35*, 325–328. [CrossRef] [PubMed]

20. Hincke, M.T.; Nys, Y.; Gautron, J.; Mann, K.; Rodriguez-Navarro, A.B.; McKee, M.D. The eggshell: Structure, composition and mineralization. *Front. Biosci.* **2012**, *17*, 1266–1280. [CrossRef]

21. Demarchi, B.; Hall, S.; Roncal-Herrero, T.; Freeman, C.L.; Woolley, J.; Crisp, M.K.; Wilson, J.; Fotakis, A.; Fischer, R.; Kessler, B.M. Protein sequences bound to mineral surfaces persist into deep time. *eLife* **2016**, *5*, e17092. [CrossRef] [PubMed]

22. Fernandez, M.S.; Moya, A.; Lopez, L.; Arias, J.L. Secretion pattern, ultrastructural localization and function of extracellular matrix molecules involved in eggshell formation. *Matrix Biol.* **2001**, *19*, 793–803. [CrossRef]

23. Nysl, Y.; Hincke, M.; Arias, J.; Garcia-Ruiz, J.; Solomon, S. Avian eggshell mineralization. *Avian Poult. Biol. Rev.* **1999**, *10*, 143–166.

24. Hincke, M.T.; Nys, Y.; Gautron, J. The role of matrix proteins in eggshell formation. *J. Poult. Sci.* **2010**, *47*, 208–219. [CrossRef]

25. Arias, J.L.; Fernandez, M.S.; Dennis, J.E.; Caplan, A.I. Collagens of the chicken eggshell membranes. *Connect. Tissue Res.* **1991**, *26*, 37–45. [CrossRef] [PubMed]

26. Panheleux, M.; Bain, M.; Fernandez, M.; Morales, I.; Gautron, J.; Arias, J.; Solomon, S.; Hincke, M.; Nys, Y. Organic matrix composition and ultrastructure of eggshell: A comparative study. *Br. Poult. Sci.* **1999**, *40*, 240–252. [CrossRef] [PubMed]

27.  Mann, K.; Maček, B.; Olsen, J.V. Proteomic analysis of the acid-soluble organic matrix of the chicken calcified eggshell layer. *Proteomics* **2006**, *6*, 3801–3810. [CrossRef] [PubMed]

28.  Rose-Martel, M.; Du, J.; Hincke, M.T. Proteomic analysis provides new insight into the chicken eggshell cuticle. *J. Proteom.* **2012**, *75*, 2697–2706. [CrossRef]

29.  Arias, J.; Fernandez, M. Role of extracellular matrix molecules in shell formation and structure. *World Poult. Sci. J.* **2001**, *57*, 349–357. [CrossRef]

30.  Rao, A.; Fernández, M.S.; Cölfen, H.; Arias, J.L. Distinct effects of avian egg derived anionic proteoglycans on the early stages of calcium carbonate mineralization. *Cryst. Growth Des.* **2015**, *15*, 2052–2056. [CrossRef]

31.  Carrino, D.A.; Rodriguez, J.P.; Caplan, A.I. Dermatan sulfate proteoglycans from the mineralized matrix of the avian eggshell. *Connect. Tissue Res.* **1997**, *36*, 175–193. [CrossRef] [PubMed]

32.  Fernandez, M.; Passalacqua, K.; Arias, J.; Arias, J. Partial biomimetic reconstitution of avian eggshell formation. *J. Struct. Biol.* **2004**, *148*, 1–10. [CrossRef] [PubMed]

33.  Mann, K.; Siedler, F. The amino sequence of ovocleidin 17, a major protein of the avian eggshell calcified layer. *IUBMB Life* **1999**, *47*, 997–1007. [CrossRef]

34.  Chien, Y.-C.; Hincke, M.; Vali, H.; McKee, M. Ultrastructural matrix–mineral relationships in avian eggshell, and effects of osteopontin on calcite growth in vitro. *J. Struct. Biol.* **2008**, *163*, 84–99. [CrossRef] [PubMed]

35.  Fernandez, M.S.; Escobar, C.; Lavelin, I.; Pines, M.; Arias, J.L. Localization of osteopontin in oviduct tissue and eggshell during different stages of the avian egg laying cycle. *J. Struct. Biol.* **2003**, *143*, 171–180. [CrossRef] [PubMed]

36.  Maroudas, A.; Mizrahi, J.; Benaim, E.; Schneiderman, R.; Grushko, G. Swelling pressure of cartilage: Roles played by proteoglycans and collagen. In *Mechanics of Swelling*; Springer: Berlin, Germany, 1992; pp. 487–512.

37.  Olszta, M.; Douglas, E.; Gower, L. Scanning electron microscopic analysis of the mineralization of type I collagen via a polymer-induced liquid-precursor (PILP) process. *Calcif. Tissue Int.* **2003**, *72*, 583–591. [CrossRef] [PubMed]

38.  Antebi, B.; Cheng, X.; Harris, J.N.; Gower, L.B.; Chen, X.-D.; Ling, J. Biomimetic collagen–hydroxyapatite composite fabricated via a novel perfusion-flow mineralization technique. *Tissue Eng. Part C Methods* **2013**, *19*, 487–496. [CrossRef] [PubMed]

39.  Gehrke, N.; Nassif, N.; Pinna, N.; Antonietti, M.; Gupta, H.S.; Cölfen, H. Retrosynthesis of nacre via amorphous precursor particles. *Chem. Mater.* **2005**, *17*, 6514–6516. [CrossRef]

40.  Hardikar, V.V.; Matijević, E. Influence of ionic and nonionic dextrans on the formation of calcium hydroxide and calcium carbonate particles. *Colloids Surfaces A Physicochem. Eng. Asp.* **2001**, *186*, 23–31. [CrossRef]

41.  Lakshminarayanan, R.; Loh, X.J.; Gayathri, S.; Sindhu, S.; Banerjee, Y.; Kini, R.M.; Valiyaveettil, S. Formation of transient amorphous calcium carbonate precursor in quail eggshell mineralization: An in vitro study. *Biomacromolecules* **2006**, *7*, 3202–3209. [CrossRef] [PubMed]

42.  Cusack, M.; Fraser, A.; Stachel, T. Magnesium and phosphorus distribution in the avian eggshell. *Comp. Biochem. Physiol. Part B Biochem. Mol. Biol.* **2003**, *134*, 63–69. [CrossRef]

43.  Wolf, S.L.; Jähme, K.; Gebauer, D. Synergy of $Mg^{2+}$ and poly(aspartic acid) in additive-controlled calcium carbonate precipitation. *CrystEngComm* **2015**, *17*, 6857–6862. [CrossRef]

44.  Sancho-Tomás, M.; Fermani, S.; Reggi, M.; García-Ruiz, J.M.; Gómez-Morales, J.; Falini, G. Polypeptide effect on $Mg^{2+}$ hydration inferred from $CaCO_3$ formation: A biomineralization study by counter-diffusion. *CrystEngComm* **2016**, *18*, 3265–3272. [CrossRef]

45.  Berg, J.K.; Jordan, T.; Binder, Y.; Börner, H.G.; Gebauer, D. $Mg^{2+}$ tunes the wettability of liquid precursors of $CaCO_3$: Toward controlling mineralization sites in hybrid materials. *J. Am. Chem. Soc.* **2013**, *135*, 12512–12515. [CrossRef] [PubMed]

46.  Liao, B.; Qiao, H.; Zhao, X.; Bao, M.; Liu, L.; Zheng, C.; Li, C.; Ning, Z. Influence of eggshell ultrastructural organization on hatchability. *Poult. Sci.* **2013**, *92*, 2236–2239. [CrossRef] [PubMed]

47.  Parsons, A. Structure of the eggshell. *Poult. Sci.* **1982**, *61*, 2013–2021. [CrossRef]

48.  Arias, J.L.; Fernández, M.A.S. Polysaccharides and proteoglycans in calcium carbonate-based biomineralization. *Chem. Rev.* **2008**, *108*, 4475–4482. [CrossRef] [PubMed]

49.  Liu, Z.; Zhang, F.; Li, L.; Li, G.; He, W.; Linhardt, R.J. Compositional analysis and structural elucidation of glycosaminoglycans in chicken eggs. *Glycoconj. J.* **2014**, *31*, 593–602. [CrossRef] [PubMed]

50.  Cha, W.I.; Hyon, S.H.; Ikada, Y. Transparent poly(vinyl alcohol) hydrogel with high water content and high strength. *Die Makromol. Chem.* **1992**, *193*, 1913–1925. [CrossRef]

51. Huang, Y.-C.; Mou, Y.; Tsai, T.W.-T.; Wu, Y.-J.; Lee, H.-K.; Huang, S.-J.; Chan, J.C. Calcium-43 NMR studies of polymorphic transition of calcite to aragonite. *J. Phys. Chem. B* **2012**, *116*, 14295–14301. [CrossRef] [PubMed]

52. Gebauer, D.; Cölfen, H.; Verch, A.; Antonietti, M. The multiple roles of additives in $CaCO_3$ crystallization: A quantitative case study. *Adv. Mater.* **2009**, *21*, 435–439. [CrossRef]

53. Huang, S.-C.; Naka, K.; Chujo, Y. A carbonate controlled-addition method for amorphous calcium carbonate spheres stabilized by poly(acrylic acid)s. *Langmuir* **2007**, *23*, 12086–12095. [CrossRef] [PubMed]

54. Xu, X.; Han, J.T.; Cho, K. Formation of amorphous calcium carbonate thin films and their role in biomineralization. *Chem. Mater.* **2004**, *16*, 1740–1746. [CrossRef]

55. Sun, S.; Mao, L.B.; Lei, Z.; Yu, S.H.; Cölfen, H. Hydrogels from amorphous calcium carbonate and polyacrylic acid: Bio-inspired materials for "mineral plastics". *Angew. Chem. Int. Ed.* **2016**, *55*, 11765–11769. [CrossRef] [PubMed]

56. Wolf, S.L.P.; Caballero, L.; Melo, F.; Cölfen, H. Gel-like calcium carbonate precursors observed by in-situ AFM. *Langmuir* **2017**, *33*, 158–163. [CrossRef] [PubMed]

57. Oaki, Y.; Kajiyama, S.; Nishimura, T.; Imai, H.; Kato, T. Nanosegregated amorphous composites of calcium carbonate and an organic polymer. *Adv. Mater.* **2008**, *20*, 3633–3637. [CrossRef]

58. Zimmerberg, J.; Kozlov, M.M. How proteins produce cellular membrane curvature. *Nat. Rev. Mol. Cell Biol.* **2006**, *7*, 9–19. [CrossRef] [PubMed]

59. Solomon, S. *Egg and Shell Quality*; Wolfe Publishing Ltd.: London, UK, 1991.

60. Bentov, S.; Weil, S.; Glazer, L.; Sagi, A.; Berman, A. Stabilization of amorphous calcium carbonate by phosphate rich organic matrix proteins and by single phosphoamino acids. *J. Struct. Biol.* **2010**, *171*, 207–215. [CrossRef] [PubMed]

61. Cölfen, H. Biomineralization: A crystal-clear view. *Nat. Mater.* **2010**, *9*, 960–961. [CrossRef] [PubMed]

62. Nudelman, F.; Pieterse, K.; George, A.; Bomans, P.H.; Friedrich, H.; Brylka, L.J.; Hilbers, P.A.; de With, G.; Sommerdijk, N.A. The role of collagen in bone apatite formation in the presence of hydroxyapatite nucleation inhibitors. *Nat. Mater.* **2010**, *9*, 1004–1009. [CrossRef] [PubMed]

63. Aizenberg, J.; Muller, D.A.; Grazul, J.L.; Hamann, D. Direct fabrication of large micropatterned single crystals. *Science* **2003**, *299*, 1205–1208. [CrossRef] [PubMed]

64. Gower, L.B.; Odom, D.J. Deposition of calcium carbonate films by a polymer-induced liquid-precursor (PILP) process. *J. Cryst. Growth* **2000**, *210*, 719–734. [CrossRef]

65. Murakami, D.; Jinnai, H.; Takahara, A. Wetting transition from the cassie–baxter state to the wenzel state on textured polymer surfaces. *Langmuir* **2014**, *30*, 2061–2067. [CrossRef] [PubMed]

66. Rao, A.; Berg, J.K.; Kellermeier, M.; Gebauer, D. Sweet on biomineralization: Effects of carbohydrates on the early stages of calcium carbonate crystallization. *Eur. J. Mineral.* **2014**, *26*, 537–552. [CrossRef]

67. Schenk, A.S.; Zope, H.; Kim, Y.-Y.; Kros, A.; Sommerdijk, N.A.; Meldrum, F.C. Polymer-induced liquid precursor (PILP) phases of calcium carbonate formed in the presence of synthetic acidic polypeptides—Relevance to biomineralization. *Faraday Discuss.* **2012**, *159*, 327–344. [CrossRef]

68. Song, R.-Q.; Cölfen, H.; Xu, A.-W.; Hartmann, J.; Antonietti, M. Polyelectrolyte-directed nanoparticle aggregation: Systematic morphogenesis of calcium carbonate by nonclassical crystallization. *Acs Nano* **2009**, *3*, 1966–1978. [CrossRef] [PubMed]

69. Song, R.Q.; Xu, A.W.; Antonietti, M.; Cölfen, H. Calcite crystals with platonic shapes and minimal surfaces. *Angew. Chem. Int. Ed.* **2009**, *48*, 395–399. [CrossRef] [PubMed]

70. De Yoreo, J.J.; Gilbert, P.U.; Sommerdijk, N.A.; Penn, R.L.; Whitelam, S.; Joester, D.; Zhang, H.; Rimer, J.D.; Navrotsky, A.; Banfield, J.F. Crystallization by particle attachment in synthetic, biogenic, and geologic environments. *Science* **2015**, *349*. [CrossRef] [PubMed]

71. Rao, A.; Cölfen, H. Mineralization schemes in the living world: Mesocrystals. In *New Perspectives on Mineral Nucleation and Growth*; Springer: Berlin, Germany, 2017; pp. 155–183.

72. Ehrlich, H.; Koutsoukos, P.G.; Demadis, K.D.; Pokrovsky, O.S. Principles of demineralization: Modern strategies for the isolation of organic frameworks: Part II. Decalcification. *Micron* **2009**, *40*, 169–193. [CrossRef] [PubMed]